

# Constraining the origin of magnetic white dwarfs

Ananya Mohapatra<sup>1†</sup> and Eric G. Blackman<sup>1,2†</sup>

<sup>1</sup>Department of Physics and Astronomy, University of Rochester, Rochester, 14627, NY, USA.

<sup>2</sup>Laboratory for Laser Energetics, University of Rochester, Rochester, 14627, NY, USA.

Contributing authors: [amohapa2@ur.rochester.edu](mailto:amohapa2@ur.rochester.edu); [eric.blackman@rochester.edu](mailto:eric.blackman@rochester.edu);

<sup>†</sup>These authors contributed equally to this work.

## Abstract

The origin of magnetic white dwarfs has been a long standing puzzle. Proposed origin mechanisms have included: fossil fields frozen in from the progenitor convective core; a dynamo in the progenitor envelope; crystallization dynamos in sufficiently cool white dwarfs; and accretion disk dynamos from white dwarf-white dwarf mergers or tidally shredded low mass stellar or planetary companions. Here we show how observational constraints on white dwarf magnetic field strengths, ages, and masses can be used to narrow down the viability of proposed origin mechanisms. Using the best available data, we find that the fossil field mechanism overpredicts the number of magnetic white dwarfs, which suggests, as supported by theoretical arguments, that the field is not actually frozen into the progenitor cores but diffuses before the white dwarfs forms. Crystallization dynamos, if operative, occur too late to explain the bulk of magnetic white dwarfs. And with progenitor envelope dynamos impeded by the theoretical challenge of depositing field from envelope to white dwarf core, the two disk dynamo mechanisms emerge as the field origin mechanisms most resilient to present constraints. The methods herein also reveal observational data gaps, and motivate future acquisition of more complete data.

**Keywords:** White Dwarfs, Dynamos, Magnetic Fields

## Main

Magnetic fields provide an external signature of internal dynamics that helps to probe the evolution of stars and compact objects. For white dwarfs (WDs), approximately 400 magnetic white dwarfs (MWDs) have been catalogued in the Montreal White Dwarf Database (MWDD), which contains about 30,000 objects [1] with magnetic fields ranging from  $\sim 10^3$  to  $\sim 10^9$  G.

Zeeman spectral line broadening and spectropolarimetry are the primary methods for measuring these WD magnetic fields [2–4]. The former provides a measure of the total magnetic field magnitude averaged over the surface of the WD  $\langle |B| \rangle$  while spectropolarimetry provides information about the average value of the signed line of sight field over the WD surface  $\langle B_z \rangle$ . Unless both techniques are available, which is more likely for cooler WDs

with fields in the range  $1 \lesssim \langle |B| \rangle \lesssim 100 \text{MG}$  [5], the values for reported magnetic fields are lower limits on the total field. If only the line of sight field is available, and the topology is assumed to be a dipole, then the total dipole field can be estimated, but this is still a lower limit on the total field.

Hardy et al. [6] analyzed hydrogen-rich MWDs using data from the MWDD supplemented by photometric and spectroscopic data from various sky surveys. The MWDD sample focuses on MWDs exhibiting Zeeman splitting, mostly indicative of magnetic field strengths  $> 1 \text{MG}$ . It reveals a notable increase in the number of MWDs starting at an approximate mass of  $0.7M_{\odot}$ , with the most massive white dwarfs (WDs) exhibiting the strongest field strengths. Overall, the origin of these magnetic fields is debated [7]. Mechanisms that have been proposed to account for MWDs can be classified into four categories: fossil fields frozen in from the progenitor convective core; crystallization dynamos; common envelope dynamos; and accretion dynamos from within common envelope or from WD/stellar mergers. Determining which of these survive evolving observational and theoretical constraints is important for constraining the physics and evolutionary pathways of WDs. Each of the mechanisms raises specific challenges to be addressed.

Ferrario and Wickramasinghe [8], review known properties of MWDs and draw connections to the properties of their progenitor main sequence stars. They argue that WD magnetic fields may arise from magnetic flux conservation during stellar evolution off the main sequence. Indeed main-sequence stars generate magnetic fields through contemporary convective dynamos, and for stellar masses greater than  $1.5M_{\odot}$  a fossil field could in principle persist in the convective core. But, as we will address, uncertainty remains as to whether the magnetic fields survive the stellar evolution all the way to the WD stage.

Complementarily, WDs undergo crystallization as they reach sufficiently low temperatures [9, 10]. As the WD solidifies into a crystalline lattice, heavier elements like  $^{12}\text{C}$  and  $^{16}\text{O}$  move towards the core, and lighter elements rise towards the outer layers, initiating a composition gradient [11]. The gravitational potential energy released is converted to the kinetic energy of buoyancy, that drive convection. This, along with WD rotation, may sustain a magnetic dynamo to amplify the magnetic field [12, 13]. Similar core crystallization has long been thought to provide an important source of free energy for outer core dynamos in planetary bodies such as Earth [14]. But we must assess how many MWDs are old enough to be consistent with the timing of crystallization onset to be explained this way.

Yet another source of free energy for MWD field amplification is differential rotation that arises when a WD core of a giant star and a companion mutually evolve. Some of this is deposited in the giant envelope, which is a possible dynamo location [15, 16]. But the necessary differential rotation free energy for a dynamo can also arise in a WD merger [17] leading to field amplification not dissimilar from that which likely occurs in neutron star mergers [18]. Alternatively, differential rotation may arise in an accretion disk formed in a tidally shredded companion during or after common envelope evolution [19–21]. These interactions provide the physical conditions where shear and magnetorotational instability driven fluctuations can generate large scale magnetic fields [22]. Even though a companion would play a key role during these amplification processes, it may be gone by the time the MWD is observed. Mergers produce isolated WDs [23] and most of the stronger MWDs are observed as isolated WDs [20]. But do these mechanisms produce sufficiently strong fields to explain all MWDs?

Here we address the above open issues raised for each of these MWD field generation scenarios and combine observational data and theoretical constraints to infer the relevance of each mechanism.

## Results

### Fossil Field Origin of MWDs is Unlikely

According to the fossil field hypothesis, the magnetic fields of MWDs observed today would be flux-frozen remnants from the progenitor main-sequence star. This presumes that magnetic flux from a core dynamo can be retained

as the WD is formed. Convective core dynamos generate magnetic fields in main-sequence stars with masses  $M/M_{\odot} > 1.5$ . For stars with  $0.5 < M/M_{\odot} < 1.5$ , convection occurs only in the envelope. Stars with  $M/M_{\odot} < 0.5$  are fully convective. The fossil field mechanism requires at least two conditions to be met. First, the WD mass must not exceed the convective core mass of the progenitor to ensure the magnetic field is generated throughout the region that becomes the WD. Second, the field must survive the formation phase of the WD. This is threatened if the conditions for dynamo growth become disfavored before the convective turbulence fully shuts down.

To address the first condition, we estimate the mass of the main sequence star from which the WD evolved. Based on the semi-empirical initial-final mass relationship described by [24], the potential progenitor star’s mass ( $M_i$ ) for each WD is calculated differently according to the WD mass categories. For WDs with masses  $M_{\text{WD}} \leq 0.6882M_{\odot}$ , the relationship is  $M_{\text{WD}} = 0.096M_i + 0.429$ . For WDs with masses  $M_{\text{WD}} > 0.6882M_{\odot}$ , the relationship is  $M_{\text{WD}} = 0.137M_i + 0.318$ . These linear relations are derived from a weighted least squares linear fit of observational data, providing a more accurate model for the initial-final mass relationship in different WD mass ranges. Figure 1a shows the mass fraction of the convective region relative to the total progenitor stellar mass [25]. We use this to compare the initial progenitor mass with the final WD mass in Figure 1b and show which WDs fall within their progenitor’s convective core mass region. The WD data are represented by blue dots, and the dashed line delineates the boundary at which WD mass equals that of its progenitor’s convective core. WDs below this line meet the condition of forming from mass entirely contained within the convective core.

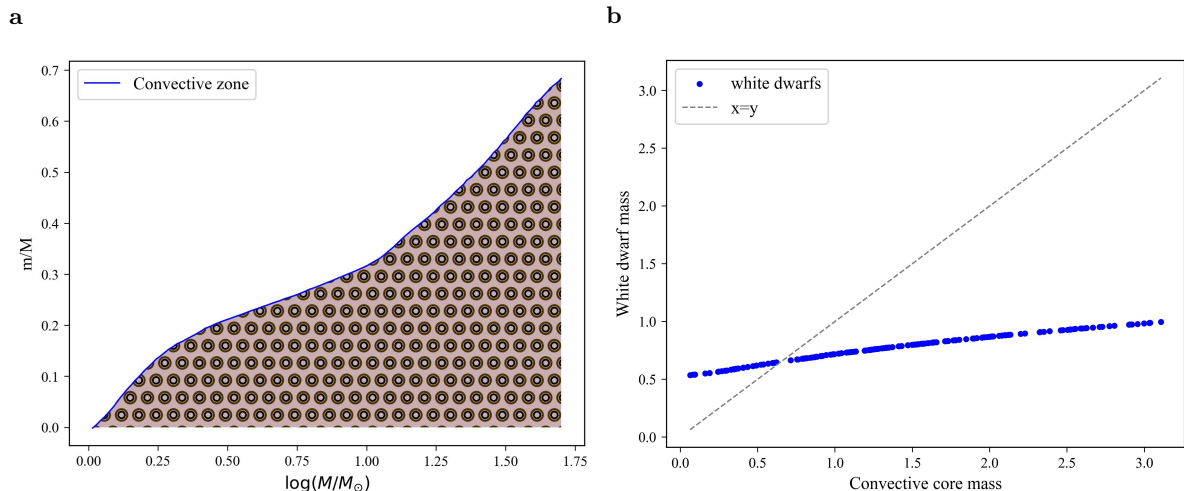


**Fig. 1: Comparison of WD Masses with Convective Core Mass** **a**, Logarithm of total mass ‘ $\log(M/M_{\odot})$ ’ versus fraction of a main sequence star’s mass within its convective core ‘ $m/M$ ’. The shaded region represents the convective zone. Adapted from figure 22.7 of Kippenhahn and Weigert. **b**, Comparison of WD masses to progenitor convective core masses (blue dots). Those WDs to the right of the  $x = y$  line fall entirely within the convective zones of their progenitors.

We next address the second condition for a viable fossil field, namely that the WD must form before the magnetic field decays. Large scale convective or turbulent dynamos require not only macroscopic transport but also a sufficiently high magnetic Reynolds number for the large-scale field stretching to overcome microphysical

dissipation. Additionally, the turbulence must maintain a field growth transport term, such as kinetic helicity, that can overcome turbulent diffusion [e.g. 26]. But as convection wanes, the system will likely transition from a turbulent, dynamo-active state which is the most demanding, to turbulent but dynamo-inactive state, and eventually to laminar flow. Even a short time in the intermediate state of turbulence without a dynamo can be important because it means turbulent diffusion without compensating growth. We must compare therefore compare the turbulent diffusion time scale to the WD formation time scale. If the former is much shorter than the latter, then survival of the fossil field is highly questionable, as the field can decay before the WD fully forms.

We estimate the turbulent diffusion timescale  $t_d$  as  $\frac{R_c^2}{D_t}$ , where  $R_c$  represents the size of the convective core, and  $D_t$  stands for the turbulent diffusion coefficient. In the context of basic mixing length theory [27], the turbulent diffusion coefficient is typically expressed as the product  $D_t = \frac{1}{3}\ell_m v_c$ , where  $\ell_m = \alpha H_p$  is the mixing length,  $v_c$  is the convective velocity, and  $\alpha$  is a dimensionless parameter that represents the ratio of the mixing length  $\ell_m$  to the pressure scale height  $H_p \approx R_c$  and characterizes the efficiency of heat transport. The velocity in the convective core is estimated as  $v_c \approx \left(\frac{F}{\rho_c}\right)^{1/3}$ , where  $F$  is the energy flux and  $\rho_c$  is the core density. We use the expressions for  $v_c$  and  $D_t$  to estimate the turbulent diffusion timescale as

$$t_d = \frac{3R_c^2}{\alpha R_c v_c} = \frac{3R_c}{\alpha \left(\frac{F}{\rho_c}\right)^{1/3}} \simeq 10.32 \text{ yr} \left(\frac{R_c}{R_\odot}\right) \left(\frac{\alpha}{0.3}\right)^{-1} \left(\frac{\rho_c}{42.65 \text{ g/cc}}\right)^{\frac{1}{3}} \left(\frac{F}{4.3 \times 10^{11} \text{ erg cm}^{-2}}\right)^{-\frac{1}{3}} \quad (1)$$

For the above numerical scaling, we used a fiducial main sequence WD progenitor mass  $M_p = 2.52M_\odot$ , from the stellar model of [28]. We scaled the energy-flux using the Stefan-Boltzmann law  $F = \sigma T_{\text{eff}}^4$ , where  $\sigma$  is the Stefan-Boltzmann constant and the effective temperature  $T_{\text{eff}} = 9332.5K$ . The resulting typical diffusion timescale  $t_d = 10.32$  years is far shorter than the estimated formation timescales of WDs, which exceed  $10^5$  yr. [29, 30]. This stark difference in timescales suggests that the fossil magnetic fields are unlikely to survive the time required for the WDs to fully form in the likely circumstance that the dynamo shuts down before convection does.

If residing below the line in Figure 1b were the only condition for a WD to retain a fossil field, that would vastly over-predict the number of magnetized WDs found in surveys. But the fact that the magnetic diffusion timescale is much shorter than the WD formation time scale plausibly explains why the fossil field mechanism is so inefficient, and likely not the dominant mechanism for WD magnetic field generation.

## Crystallization Dynamo May Explain at most a Minority of MWDs

The exact temperature evolution of WD crystallization depends on the thermodynamic properties and composition of the WD, including the ratio of carbon to oxygen. For typical WDs, crystallization is expected to take place within a temperature range of approximately  $10^4 - 10^5K$  [31]. We can rule out crystallization dynamos as the primary explanation for MWDs younger than the age of crystallization, and check for evidence of an increase in MWDs after crystallization [32]. To determine crystallization ages, we use the theoretical evolutionary sequences of Bédard et al.[33]. These sequences<sup>1</sup> translate the effective WD temperature into a cooling age. We use these cooling models to construct temperature-age cooling curves [34] for different WD masses, determine the corresponding ages of crystallization [35], and compare these to the observed MWDs.

---

<sup>1</sup>accessible online at <http://www.astro.umontreal.ca/bergeron/CoolingModels/> under the section titled ‘Evolutionary Sequences’

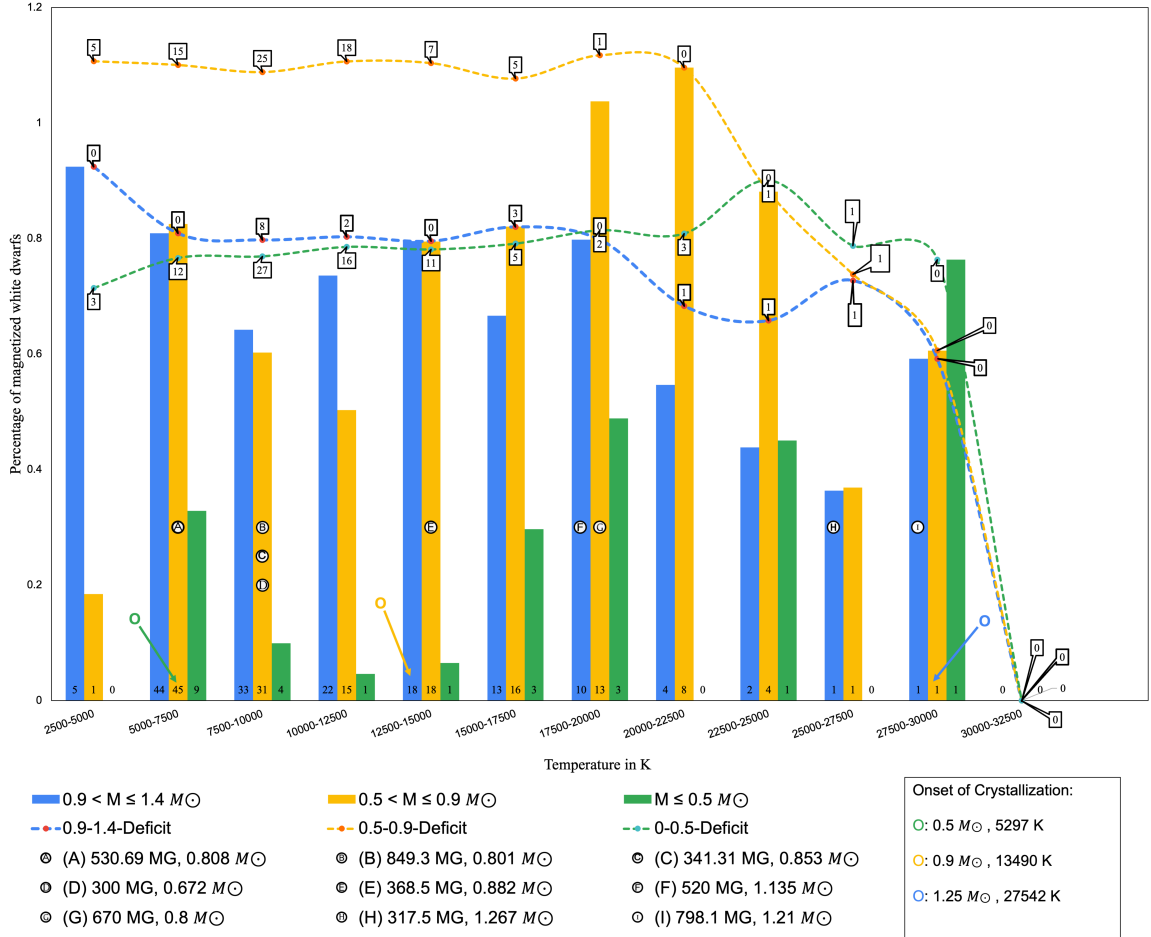


**Fig. 2: Percentage of white dwarfs magnetized in different mass ranges.** Histogram depicting the percentage of MWDs in a range of temperature bins from younger to older, as temperatures decrease. Colored dotted lines show estimates of the deficit in that bin to make the fraction of MWDs constant with age. Objects marked A-I represent high field MWDs ( $> 300$  MG).

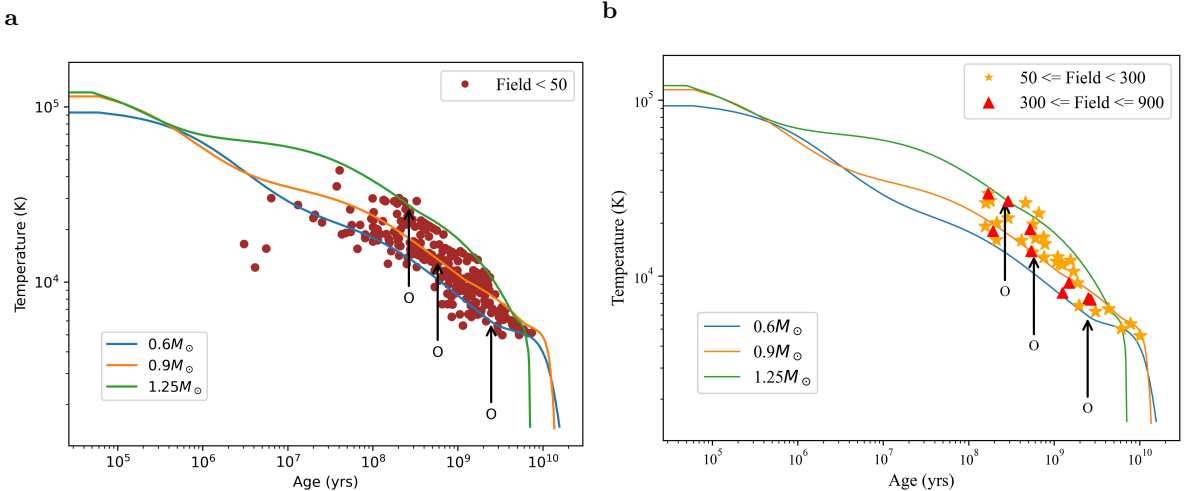


**Fig. 3: Cooling curves for 3 distinct WD masses, with the onset of crystallization marked. a**, WDs with field strengths below 50 MG. **b**, WDs with field strengths between 50–300 MG and 300–900 MG, showing their positions relative to the onset of crystallization.

Figure 2 shows a histogram of the percentage of MWDs within temperature bins, with three different colors representing three distinct mass ranges. Each mass category includes dotted lines estimating the deficit of MWDs needed to maintain at least a constant fraction of MWDs relative to the total WDs over time. To best understand this, begin at the rightmost part of the plot for a given color bar, say blue, and follow the blue dotted line to the left, which corresponds to increasing age. In the right-most temperature bin there is 1 MWD in the blue bin. Moving to the second temperature bin from right to left, there is also 1 MWD. The number in the box above that bin at the blue dotted line is 1, indicating that 1 additional MWD would be needed to keep the fraction of MWDs constant. Moving another bin to the left, the number on the blue dotted line is again 1, meaning an additional MWD is missing if the MWDs to WDs fraction were to remain constant from the original rightmost bin. The interpretation applies similarly to the green and yellow dotted lines for their respective colored mass range bars as one progresses from right to left temperature bins. The higher mass range (blue) histogram generally shows much less of a WD deficit needed to maintain a constant fraction, compared to the the lower mass range MWDs. Assuming that the magnetic fields do not decay substantially on cooling time scales between temperature bins, this suggests that substantial numbers of MWDs are missing from what would be a complete observational sample.

High field MWDs with field strengths greater than 300 MG are marked in Figure 2 with letters A through I within their respective mass categories, indicating their positions in temperature. The crystallization arrows show the onset of crystallization for certain WD masses. The onset temperatures increase with mass, and the range for the entire mass range can be inferred by interpolation. This also allows for a direct comparison with the crystallization curves in Figure 3, which depict three cooling curves corresponding to different masses, with the onset of crystallization marked to compare with the WD cooling ages. In Figure 3a we show MWDs with field strengths below 50 MG along these curves, relative to the onset of crystallization. Only MWD older than the age of crystallization onset could have been influenced by the crystallization dynamo. Figure 3b presents

similar cooling curves but for two different ranges of field strengths, 50 – 300 MG and 300 – 900 MG, marked with different symbols.

Overall, the data and plots reveal a notable increase in the fraction of magnetized WDs within the temperature range 5000-7500K, suggesting a potential link to the crystallization dynamo. This is further evidenced by the cooling curves in Figure 3, which show where the high field MWDs appear relative to the crystallization onset for different mass ranges. So despite the limited availability of data, as evidenced by the deficits indicated in Figure 2, crystallization cannot therefore be ruled out as an influence on magnetic field generation. However, given the presence of numerous magnetized WDs before the onset of crystallization it cannot be primary mechanism responsible for the magnetic fields of most MWDs.

### The trouble with envelope dynamos

Dynamos in giant stellar envelopes are another possible source of free energy to generate magnetic fields that could in principle be used for the magnetic fields of WD. In particular, large-scale magnetic field amplification in the envelope of the giant star during a common envelope (CE) phase has been studied [15, 36–38]. The CE phase typically occurs when a red giant or asymptotic giant branch star engulfs a companion. As the companion star in-spirals, it transfers orbital energy and angular momentum to the envelope, that causes differential rotation and thus a source of free energy in shear. Because the envelopes of giant stars are strongly convective, conditions for an  $\alpha - \Omega$  type dynamo are favorable, with the highest amplification at the interface between the convective and radiative regions, where the shear is strongest.

However, as the CE phase progresses and the envelope is drained, the mechanism faces challenges [20]. To reach the WD surface, the magnetic fields must diffuse or be pumped downward through the layers of the evolving star while the envelope is expanding and escaping outward. Moreover, the envelope dynamo operates only transiently during the CE phase. For the magnetic fields to be inherited by the WD, they must be available for deposit until the WD fully forms. Unless these challenges can be convincingly resolved, these models are unlikely to be the dominant source of MWDs.

### Accretion Dynamos are the most plausible source of most MWDs

The merger of two WDs gives rise to a remnant comprising a central WD and a surrounding hot disk or torus formed from approximately half of the disrupted secondary star [39]. Within this accretion torus, convection and differential rotation may drive a large scale “ $\alpha - \Omega$ ” or “ $\alpha^2 - \Omega$ ” type dynamo. Simulations and analytic estimates suggest that resulting magnetic field strengths could range from  $10^7 - 10^{10}$  G [40]. An accretion disk around a WD can also form from CE interaction if a low mass companion star or planet is tidally disrupted by the WD core of the primary giant star [19, 41]. WD fields can result from accreting the magnetized material [20]. Since both WD-WD mergers and tidal shredding of a companion lead to accretion disks, we can conceptually unify these two mechanisms in estimating the magnetic field strength they may impart to the WD.

To estimate the total and poloidal field strengths that result from accretion and compare them to values observed in the MWD population, we consider companion masses ( $M_c$ ) ranging from sub-Jupiter-mass ( $< M_J$ ) planets to low-mass stars and first estimate the fields generated by a dynamo operating within the associated disk. An accretion dynamo operates within the disk of shredded companion material, and can survive evaporation within the envelope to accrete flux, [41]. MRI turbulence for example, [42] can amplify the magnetic field and source the transport coefficients for a large scale  $\alpha - \Omega$ -type dynamo in a stratified disk.

We assume a standard accretion disk model [43, 44] for which the mean fields and flows are axisymmetric, with turbulent transport supplied by the MRI [e.g. 45]. The Alfvén speed at each radius,  $R$  for the total field in an MRI-saturated disk can be estimated from  $\alpha_{ss}\beta \sim 0.1$  [46], where  $\beta$  is the ratio of thermal to magnetic

pressure, and  $\alpha_{ss}$  is the Shakura-Sunyaev dimensionless parameter quantifying the turbulent stress that transports angular momentum. Typically,  $0.0001 \leq \alpha_{ss} \leq 0.1$  as measured in simulations or inferred from observations. Since the magnitude of the mean field dynamo-generated mean magnetic field in the disk is less than the total field magnitude, we have a relationship  $\alpha_{ss}\beta(\bar{v}_A) \geq 0.1$  which implies that the squared Alfvén speed for the mean field is approximately  $\bar{v}_A^2 \leq 20\alpha_{ss}c_s^2$  [47], where the overline denotes quantities associated with the mean magnetic field. Here,  $c_s$  is the sound speed which, from hydrostatic equilibrium, can also be expressed as the product  $c_s \simeq H\Omega_k$  where  $H$  is the disk scale height,  $\Omega_k$  is the Keplerian orbital frequency. From local mass conservation, the mass density of the in terms of the local accretion rate  $\dot{M}$  is

$$\rho = \frac{\dot{M}}{4\pi HR\bar{v}_R} = \frac{\dot{M}}{4\pi H^3\alpha_{ss}\Omega_k}, \quad (2)$$

where  $\bar{v}_R \simeq \alpha_{ss}c_s H/R$  is the radial accretion speed. We will make use equation (2) exclusively at the inner edge of the disk. We use the total magnetic field  $B_d$  as an upper limit for the mean toroidal field  $\bar{B}_\phi$ , which dominates the mean. Combining the  $\alpha_{ss}\beta \sim 0.1$  relation with equation (2) we then obtain

$$\bar{B}_\phi \leq B_d \simeq (80\pi\rho c_s^2\alpha_{ss})^{1/2} = 4.47 \left( \frac{\dot{M}\Omega_k}{H} \right)^{1/2}. \quad (3)$$

The mean poloidal field,  $\bar{B}_p$  is related to the mean toroidal field  $\bar{B}_\phi$  according to  $\bar{B}_p = \alpha_{ss}^{1/2}\bar{B}_\phi$  [47]. We can estimate this at the innermost radius of a WD accretion disk, assuming that the inner edge of the disk extends close to the WD radius. Scaled for a WD of mass  $M_{WD}$  and radius  $R_{WD}$ , this gives

$$\bar{B}_p \lesssim \alpha_{ss}^{1/2} \left( \frac{\dot{M}\Omega_k}{H} \right)^{1/2} \approx 22.62 \text{ MG} \left( \frac{\eta_{ac}}{0.1} \right)^{1/2} \left( \frac{\alpha_{ss}}{10^{-2}} \right) \left( \frac{M_c}{30M_J} \right)^{3/4} \left( \frac{M_{WD}}{0.6M_\odot} \right)^{1/4} \left( \frac{r_c}{r_J} \right)^{-1/4} \left( \frac{H/R}{0.05} \right)^{1/2} \left( \frac{R}{10^9 \text{ cm}} \right)^{-3/4}, \quad (4)$$

where we have used the accretion rate from viscous angular momentum transport given by [20]

$$\dot{M} \sim 0.07 M_{\odot} \text{yr}^{-1} \left( \frac{\tilde{\eta}}{0.1} \right) \left( \frac{\alpha_{ss}}{10^{-2}} \right) \left( \frac{H/R}{0.05} \right)^2, \quad (5)$$

and  $\tilde{\eta} = \eta_{ac} \left( \frac{M_c}{30M_J} \right)^{-3/2} \left( \frac{r_c}{r_J} \right)^{1/2}$ , where  $r_J$  is a Jupiter radius. Here  $\eta_{ac}$  is an efficiency parameter that is smaller when more mass is lost to outflows. We consider only companions with  $M_c \leq 500M_J$ . Our use of  $\tilde{\eta}$  allows us to control the accretion rate in a form that is independent of planet mass and radius in what follows. The aspect ratio  $H/R$  in equation (5) denotes the scale height of the accretion disk relative to its radius and is calculated from hydrostatic equilibrium as

$$\frac{H}{R} = \frac{\sqrt{kT/m_p}}{\sqrt{GM_{WD}/R_{WD}}} = \left( \frac{k}{\mu m_p} \right)^{1/2} \left( \frac{3}{\sigma} \frac{\dot{M}R_{WD}}{G^3 M_{WD}^3} \right)^{1/8} = 0.0367 \left( \frac{M_{WD}}{0.6M_\odot} \right)^{-3/8} \left( \frac{\dot{M}}{\dot{M}_{ed}} \right)^{1/8} \left( \frac{R_{WD}}{10^9 \text{ cm}} \right)^{1/8}, \quad (6)$$

where  $T \simeq \frac{3GM\dot{M}}{8\pi\sigma}$  was used as the temperature for the accretion disk [44],  $m_p$  is the proton mass,  $k$  the Boltzmann constant,  $\mu$  is the mean molecular weight, and  $G$  is the gravitational constant. This aspect ratio is only weakly sensitive to the accretion rate.



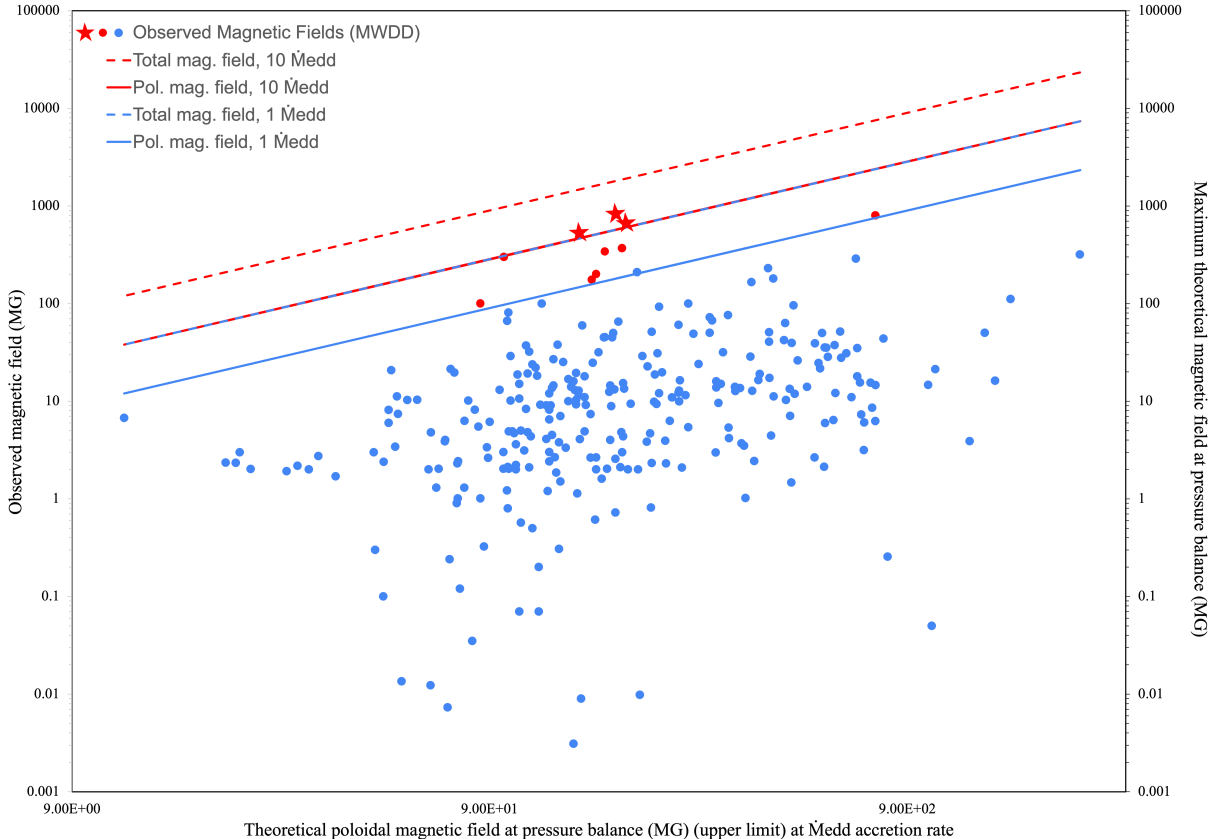


**Fig. 4: Comparison of Observed and Theoretical White Dwarf Magnetic Fields.** The plot shows observed magnetic field strengths (y-axis) versus theoretical limits (x-axis) for magnetic white dwarfs. Dots and stars represent MWDDs with different field strength ranges, with theoretical limits indicated in the legend. Solid and dashed lines denote the theoretical upper limits of poloidal and total magnetic field strength respectively, as derived in the text. The blue dashed line, overlaps exactly with the red solid line.

Accretion of a shredded companion and magnetic field onto a WD at the initial accretion rate could continue for about a viscous time scale, unless the accumulated stress from the total WD magnetic field,  $B_{\text{WD}}$  counterbalances the Keplerian ram stress exerted by the orbiting material in the disk first. As we now show, this balance does indeed occur before a viscous time, and therefore provides the limiting field. Using pressure balance as a rough proxy for stress balance [47], the magnetic pressure  $\frac{B_{\text{WD}}^2}{8\pi}$  balances the Keplerian ram pressure  $\rho V_k^2$  where  $V_k$  is the Keplerian velocity at the disk, at a field strength of

$$B_{\text{WD}} \leq \sqrt{8\pi\rho V_k^2}. \quad (7)$$

On the other hand, the magnetic field strength advected over a viscous accretion time, when transported at a rate determined by free fall time, or the Keplerian orbital frequency  $\Omega_k$  at the disk's inner radius  $\sim R_{\text{WD}}$ , would be

$$B_{\text{WD}} \leq B_d \Omega_k (R_{\text{WD}}) t_v. \quad (8)$$

To compare equations (7) and (8), we need expressions for  $B_d$  and  $t_v$ . From equation (3), we have  $B_d \geq 8.94\sqrt{\pi\rho\alpha_{\text{ss}}c_s}$ . The viscous timescale is given by  $t_v = \frac{R^2}{\nu_T} \simeq \frac{R_{\text{WD}}^2}{\alpha_{\text{ss}}c_s H}$ , where we have used the effective turbulent viscosity  $\nu_T = \alpha_{\text{ss}}c_s H$ , and  $R \sim R_{\text{WD}}$  as the disk radius where the time scale is evaluated. Combining these into equation (8), the estimated total field accumulated viscously in  $t_v$  would be

$$B_{\text{WD}}(t_v) = 8.94\sqrt{\pi\rho} \frac{(\Omega_k R_{\text{WD}}) R_{\text{WD}}}{\sqrt{\alpha_{\text{ss}}H}} = 15.87\sqrt{\rho V_k^2} \frac{R_{\text{WD}}}{\sqrt{\alpha_{\text{ss}}H}}. \quad (9)$$

The inequality  $\frac{R_{\text{WD}}}{\sqrt{\alpha_{\text{ss}}H}} > 1$  always holds, which implies that the magnetic field accumulated always exceeds the pressure-limited threshold of equation (7). Therefore, the pressure balance limits the WD magnetic field to the value given by equation (7).

As emphasized earlier, the observational methods often provide a lower limit to the total magnetic field strength estimated theoretically. In cases where the toroidal magnetic field is undetectable, the reported observed field strengths may more closely reflect the net signed poloidal field. In figure 4 we therefore compare the observationally reported MWD fields to the maximum total WD magnetic fields predicted by pressure equilibrium (dotted lines) as well as the maximum poloidal fields (solid lines) associated with this equilibrium. To establish the pressure-limited magnetic field value, we use equations (2), (7) and  $V_k = \sqrt{\frac{GM}{R}}$  at  $R \sim R_{\text{WD}}$ . We set  $\dot{M}$  onto the WD to be a multiple of the Eddington rate of  $\dot{M}_{\text{ed}} = L_{\text{ed}}/V_k^2 = 10^{-5}M_{\odot}\text{yr}^{-1}$  for  $R_{\text{WD}} = 10^9\text{cm}$ , and  $\alpha_{\text{ss}} = 0.1$ ; any smaller  $\alpha$  would produce even higher lines making this choice a conservative one. The dependence on  $1/\alpha_{\text{ss}}^{1/2}$  for the lines corresponding to the total field arise from equation (2), since we choose a fixed accretion rate. The poloidal field lines are independent of  $\alpha_{\text{ss}}$  as the poloidal field is reduced from the total by  $\alpha_{\text{ss}}^{1/2}$ .

The blue lines on the plot correspond to  $\dot{M} = \dot{M}_{\text{ed}}$  and the red lines correspond to  $\dot{M} = 10\dot{M}_{\text{ed}}$ . The dashed lines correspond to the total field limit and the solid lines to the poloidal field. The multicolored middle line results because the blue dashed line overlaps exactly with the red solid line. Observed MWD fields are shown as dots and stars: blue dots indicate WDs with fields below the blue solid line; red dots indicate WDs with fields above the blue solid line but below the red solid line; and red stars represent WDs that lie below only the red dashed line. This analysis reveals that the estimated WD magnetic fields, derived from pressure equilibrium in an accretion scenario, can in principle explain the observed WD field strengths using plausible accretion rates  $\dot{M} \leq 10\dot{M}_{\text{ed}}$ .

## Discussion

Our analysis constrains the viable proposed mechanisms for MWDs when examined against existing observational and theoretical constraints. Accretion-driven dynamo mechanisms from tidally shredded companions or WD mergers are the hardest to presently rule out as an explanation for the magnetic fields in most MWDs, as summarized in Figure 4. More detailed theoretical investigation of accretion based models is particularly warranted, both to better understand the field generation in the disk and advection of the field onto the WD. And, as more data become available, the position of new WDs on updated versions of Figure 4 will help to further constrain the plausibility of these mechanisms. In contrast, the hypothesis that magnetic fields in WDs are flux-frozen relics

from progenitor stars seems unlikely, given that the progenitor turbulent diffusion timescales are much shorter than the WD formation timescale.

In addition, our comparison of MWD cooling ages compared to the theoretically expected crystallization onset ages reveals that crystallization occurs too late to be the dominant mechanism for magnetic field generation in the majority of MWDs. The analysis does however reveal the potential role for crystallization dynamos for some older cooler WD, particularly MWDs in the 5000-7500 K, range, and more data are needed to pin down this subset of systems. The incompleteness of current MWD data is evidenced by the fact that the fraction of MWDs as a function of cooling age decreases with WD age for large sections of Figure 2, which would not occur if the sample were complete. Our results and methodology highlight the importance of acquiring more complete data sets.

## Acknowledgements

We thank I. Caiazzo, J. Fuller, J. Nordhaus, L. Chamandy, and S. Ginzburg for related discussions. We acknowledge partial support from grants NSF PHY-2020249, and the Aspen Center for Physics, which is supported by National Science Foundation grant PHY-2210452. We acknowledge support by the U.S DOE NNSA under Awards DE-NA0003856 and DE-NA0003842, DE-NA0004147, DE-NA0004144, and Subcontracts 536203 and 630138 with LANL and B632670 with LLNL through the Flash Center for Computational Science. Support from the U.S. DOE ARPA-E under Award DE-AR0001272 and U.S. DOE Office of Science, Fusion Energy Sciences under Award DE-SC0021990 is also acknowledged.

## Data Availability

Data sources used for this analysis are cited in the text.

## Declarations

### Ethics declarations

Competing interests- The authors declare no competing interests.

## References

- [1] Dufour, P., Blouin, S., Coutu, S., Fortin-Archambault, M., Thibeault, C., Bergeron, P., Fontaine, G.: The Montreal White Dwarf Database: A Tool for the Community. In: Tremblay, P.-E., Gaensicke, B., Marsh, T. (eds.) 20th European White Dwarf Workshop. Astronomical Society of the Pacific Conference Series, vol. 509, p. 3 (2017). <https://doi.org/10.48550/arXiv.1610.00986>
- [2] Berdyugin, A.V., Piirola, V., Bagnulo, S., Landstreet, J.D., Berdyugina, S.V.: Highly sensitive search for magnetic fields in white dwarfs using broad-band circular polarimetry. *A&A* **657**, 105 (2022) <https://doi.org/10.1051/0004-6361/202142173> [arXiv:2111.11174](https://arxiv.org/abs/2111.11174) [astro-ph.SR]
- [3] Berdyugin, Andrei V., Piirola, Vilppu, Bagnulo, Stefano, Landstreet, John D., Berdyugina, Svetlana V.: Discovery of magnetic fields in five dc white dwarfs. *A&A* **670**, 2 (2023) <https://doi.org/10.1051/0004-6361/202245149>

- [4] Berdyugin, A., Landstreet, J.D., Bagnulo, S., Pirola, V., Berdyugina, S.V.: Searching for magnetic fields in featureless white dwarfs with the DIPOL-UF polarimeter at the Nordic Optical Telescope (2024). <https://arxiv.org/abs/2408.03614>
- [5] Bagnulo, Stefano, Landstreet, John D.: Discovery of six new strongly magnetic white dwarfs in the 20 pc local population. *A&A* **643**, 134 (2020) <https://doi.org/10.1051/0004-6361/202038565>
- [6] Hardy, F., Dufour, P., Jordan, S.: Spectrophotometric analysis of magnetic white dwarf – i. hydrogen-rich compositions. *Monthly Notices of the Royal Astronomical Society* **520**(4), 6111–6134 (2023) <https://doi.org/10.1093/mnras/stad196>
- [7] Bagnulo, S., Landstreet, J.D.: Multiple channels for the onset of magnetism in isolated white dwarfs. *The Astrophysical Journal Letters* **935**(1), 12 (2022) <https://doi.org/10.3847/2041-8213/ac84d3>
- [8] Ferrario, L., Wickramasinghe, D.T.: Magnetic fields and rotation in white dwarfs and neutron stars. *MNRAS* **356**(2), 615–620 (2005) <https://doi.org/10.1111/j.1365-2966.2004.08474.x>
- [9] Kirzhnits, D.: Internal structure of super-dense stars. *Sov. Phys. JETP* **11**, 365–368 (1960)
- [10] Van Horn, H.: Crystallization of white dwarfs. *Astrophysical Journal*, vol. 151, p. 227 **151**, 227 (1968)
- [11] Stevenson, D.: A eutectic in carbon-oxygen white dwarfs? *Le Journal de Physique Colloques* **41**(C2), 2–61 (1980)
- [12] Ginzburg, S., Fuller, J., Kawka, A., Caiazzo, I.: Slow convection and fast rotation in crystallization-driven white dwarf dynamos. *Monthly Notices of the Royal Astronomical Society* **514**(3), 4111–4119 (2022) <https://doi.org/10.1093/mnras/stac1363>
- [13] Fuentes, J.R., Castro-Tapia, M., Cumming, A.: A Short Intense Dynamo at the Onset of Crystallization in White Dwarfs. *ApJ* **964**(1), 15 (2024) <https://doi.org/10.3847/2041-8213/ad3100> [arXiv:2402.03639](https://arxiv.org/abs/2402.03639) [astro-ph.SR]
- [14] Isern, J., García-Berro, E., Külebi, B., Lorén-Aguilar, P.: A common origin of magnetism from planets to white dwarfs. *The Astrophysical Journal Letters* **836**(2), 28 (2017) <https://doi.org/10.3847/2041-8213/aa5eae>
- [15] Tout, C.A., Wickramasinghe, D.T., Liebert, J., Ferrario, L., Pringle, J.E.: Binary star origin of high field magnetic white dwarfs. *MNRAS* **387**(2), 897–901 (2008) <https://doi.org/10.1111/j.1365-2966.2008.13291.x> [arXiv:0805.0115](https://arxiv.org/abs/0805.0115) [astro-ph]
- [16] Roepke, F.K., Marco, O.D.: Simulations of common-envelope evolution in binary stellar systems: physical models and numerical techniques (2022). <https://arxiv.org/abs/2212.07308>
- [17] Wickramasinghe, D.T., Tout, C.A., Ferrario, L.: The most magnetic stars. *Monthly Notices of the Royal Astronomical Society* **437**(1), 675–681 (2013) <https://doi.org/10.1093/mnras/stt1910> <https://academic.oup.com/mnras/article-pdf/437/1/675/18457709/stt1910.pdf>
- [18] Kiuchi, K., Reboul-Salze, A., Shibata, M., Sekiguchi, Y.: A large-scale magnetic field produced by a solar-like dynamo in binary neutron star mergers. *Nature Astronomy* **8**, 298–307 (2024) <https://doi.org/10.1038/>

s41550-024-02194-y arXiv:2306.15721 [astro-ph.HE]

- [19] Nordhaus, J., Blackman, E.G.: Low-mass binary-induced outflows from asymptotic giant branch stars. *MNRAS* **370**(4), 2004–2012 (2006) <https://doi.org/10.1111/j.1365-2966.2006.10625.x> arXiv:astro-ph/0604445 [astro-ph]
- [20] Nordhaus, J., Wellons, S., Spiegel, D.S., Metzger, B.D., Blackman, E.G.: Formation of high-field magnetic white dwarfs from common envelopes. *Proceedings of the National Academy of Science* **108**(8), 3135–3140 (2011) <https://doi.org/10.1073/pnas.1015005108> arXiv:1010.1529 [astro-ph.SR]
- [21] Ondratschek, P.A., Röpke, F.K., Schneider, F.R.N., Fendt, C., Sand, C., Ohlmann, S.T., Pakmor, R., Springel, V.: Bipolar planetary nebulae from common-envelope evolution of binary stars. *A&A* **660**, 8 (2022) <https://doi.org/10.1051/0004-6361/202142478> arXiv:2110.13177 [astro-ph.SR]
- [22] Bhat, P., Ebrahimi, F., Blackman, E.G.: Large-scale dynamo action precedes turbulence in shearing box simulations of the magnetorotational instability. *Monthly Notices of the Royal Astronomical Society* **462**(1), 818–829 (2016) <https://doi.org/10.1093/mnras/stw1619> <https://academic.oup.com/mnras/article-pdf/462/1/818/18470481/stw1619.pdf>
- [23] Briggs, G.P., Ferrario, L., Tout, C.A., Wickramasinghe, D.T., Hurley, J.R.: Merging binary stars and the magnetic white dwarfs. *Monthly Notices of the Royal Astronomical Society* **447**(2), 1713–1723 (2014) <https://doi.org/10.1093/mnras/stu2539>
- [24] Catalán, S., Isern, J., García-Berro, E., Ribas, I.: The initial-final mass relationship of white dwarfs revisited: effect on the luminosity function and mass distribution. *MNRAS* **387**(4), 1693–1706 (2008) <https://doi.org/10.1111/j.1365-2966.2008.13356.x> arXiv:0804.3034 [astro-ph]
- [25] Kippenhahn, R., Weigert, A.: *Stellar Structure and Evolution*, (1990)
- [26] Brandenburg, A., Subramanian, K.: Astrophysical magnetic fields and nonlinear dynamo theory. *Physics Reports* **417**(1–4), 1–209 (2005) <https://doi.org/10.1016/j.physrep.2005.06.005>
- [27] Shu, F.H.: *The Physics of Astrophysics. Volume II: Gas Dynamics.*, (1992)
- [28] Mowlavi, N., Eggenberger, P., Meynet, G., Ekström, S., Georgy, C., Maeder, A., Charbonnel, C., Eyer, L.: Stellar mass and age determinations . I. Grids of stellar models from  $Z = 0.006$  to  $0.04$  and  $M = 0.5$  to  $3.5 M_{\odot}$ . *A&A* **541**, 41 (2012) <https://doi.org/10.1051/0004-6361/201117749> arXiv:1201.3628 [astro-ph.SR]
- [29] Vila, S.C.: Pre-White-Dwarf Evolution. I. *ApJ* **146**, 437 (1966) <https://doi.org/10.1086/148908>
- [30] Vila, S.C.: Pre-White-Dwarf Evolution. II. *ApJ* **149**, 613 (1967) <https://doi.org/10.1086/149289>
- [31] Schreiber, M., Belloni, D., Gänsicke, B., Parsons, S., Zorotovic, M.: The origin and evolution of magnetic white dwarfs in close binary stars. *Nature Astronomy* **5**, 1–7 (2021) <https://doi.org/10.1038/s41550-021-01346-8>
- [32] Blatman, D., Ginzburg, S.: Magnetic field breakout from white dwarf crystallization dynamos. *Monthly Notices of the Royal Astronomical Society* **528**(2), 3153–3162 (2024) <https://doi.org/10.1093/mnras/stae222> <https://academic.oup.com/mnras/article-pdf/528/2/3153/56544140/stae222.pdf>

- [33] Bédard, A., Bergeron, P., Brassard, P., Fontaine, G.: On the Spectral Evolution of Hot White Dwarf Stars. I. A Detailed Model Atmosphere Analysis of Hot White Dwarfs from SDSS DR12. *ApJ* **901**(2), 93 (2020) <https://doi.org/10.3847/1538-4357/abafbe> arXiv:2008.07469 [astro-ph.SR]
- [34] Ginzburg, S.: Younger age for the oldest magnetic white dwarfs (2024). <https://arxiv.org/abs/2408.04695>
- [35] Tremblay, P.-E., Fontaine, G., Fusillo, N.P.G., Dunlap, B.H., Gänsicke, B.T., Hollands, M.A., Hermes, J.J., Marsh, T.R., Cukanovaite, E., Cunningham, T.: Core crystallization and pile-up in the cooling sequence of evolving white dwarfs. *Nature* **565**(7738), 202–205 (2019) <https://doi.org/10.1038/s41586-018-0791-x>
- [36] Regós, E., Tout, C.A.: The effect of magnetic fields in common-envelope evolution on the formation of cataclysmic variables. *MNRAS* **273**(1), 146–156 (1995) <https://doi.org/10.1093/mnras/273.1.146>
- [37] Nordhaus, J., Blackman, E.G., Frank, A.: Isolated versus common envelope dynamos in planetary nebula progenitors. *MNRAS* **376**(2), 599–608 (2007) <https://doi.org/10.1111/j.1365-2966.2007.11417.x> arXiv:astro-ph/0609726 [astro-ph]
- [38] Kissin, Y., Thompson, C.: Spin and Magnetism of White Dwarfs. *ApJ* **809**(2), 108 (2015) <https://doi.org/10.1088/0004-637X/809/2/108> arXiv:1501.07197 [astro-ph.SR]
- [39] Garcia-Berro, E., Torres, S., Lorén-Aguilar, P., Aznar Siguan, G., Camacho, J., Külebi, B., Isern, J., Althaus, L., Córscico, A.: On the origin of high-field magnetic white dwarfs, 423 (2013)
- [40] García-Berro, E., Lorén-Aguilar, P., Aznar-Siguán, G., Torres, S., Camacho, J., Althaus, L.G., Córscico, A.H., Külebi, B., Isern, J.: Double Degenerate Mergers as Progenitors of High-field Magnetic White Dwarfs. *ApJ* **749**(1), 25 (2012) <https://doi.org/10.1088/0004-637X/749/1/25> arXiv:1202.0461 [astro-ph.SR]
- [41] Guidarelli, G., Nordhaus, J., Chamandy, L., Chen, Z., Blackman, E.G., Frank, A., Carroll-Nellenback, J., Liu, B.: Hydrodynamic simulations of disrupted planetary accretion discs inside the core of an AGB star. *MNRAS* **490**(1), 1179–1185 (2019) <https://doi.org/10.1093/mnras/stz2641> arXiv:1908.00157 [astro-ph.SR]
- [42] Salmeron, R., Königl, A., Wardle, M.: Angular momentum transport in protostellar discs. *MNRAS* **375**(1), 177–183 (2007) <https://doi.org/10.1111/j.1365-2966.2006.11277.x> arXiv:astro-ph/0611359 [astro-ph]
- [43] Shakura, N.I., Sunyaev, R.A.: Black holes in binary systems. Observational appearance. *A&A* **24**, 337–355 (1973)
- [44] Frank, J., King, A., Raine, D.: *Accretion Power in Astrophysics*, 3rd edn. Cambridge University Press, ??? (2002)
- [45] Balbus, S.A., Hawley, J.F.: Instability, turbulence, and enhanced transport in accretion disks. *Reviews of Modern Physics* **70**(1), 1–53 (1998) <https://doi.org/10.1103/RevModPhys.70.1>
- [46] Blackman, E.G., Penna, R.F., Varnière, P.: Empirical relation between angular momentum transport and thermal-to-magnetic pressure ratio in shearing box simulations. *New Astron.* **13**(4), 244–251 (2008) <https://doi.org/10.1016/j.newast.2007.10.004> arXiv:astro-ph/0607119 [astro-ph]
- [47] Blackman, E.G., Frank, A., Welch, C.: Magnetohydrodynamic stellar and disk winds: Application to planetary

nebulae. *The Astrophysical Journal* **546**(1), 288-298 (2001) <https://doi.org/10.1086/318253>